Magnetophotorefractive effects in diluted magnetic semiconductors: Theory and experiment

R. S. Rana,* Eunsoon Oh, K. Chua, A. K. Ramdas, and D. D. Nolte
Department of Physics, Purdue University, West Lafayette, Indiana 47907
(Received 8 November 1993)

Faraday and Voigt magneto-optic effects in undoped $Cd_{1-x}Mn_xTe$, a diluted magnetic semiconductor, modify nonlinear beam coupling during photorefractive two-wave mixing. Three magnetophotorefractive geometries using transmission holographic gratings are identified: (1) the longitudinal Faraday geometry; (2) the transverse Faraday geometry; and (3) the Voigt geometry. In the magnetophotorefractive phenomena, magnetic-field-induced circular and linear birefringence alters the polarization and phase of coupled modes propagating in the presence of electro-optic gratings generated by photoinduced space charge. Experimental and theoretical behavior for each of the geometries is presented as functions of incident beam polarization and magnetic-field strength. The magnetic field controls the magnitude and the direction of nonreciprocal energy transfer between the two beams.

I. INTRODUCTION

The photorefractive effect is a dynamic holographic process in which laser interference fringes are imprinted in the material as a refractive index grating.[1,2] Such a grating can couple two coherent laser beams during two-wave mixing, leading to a nonreciprocal energy transfer with one beam gaining intensity at the expense of the other.[1–4] The photorefractive grating formation is a three-step process involving the generation of photocarriers, the development of space-charge electric fields, and an electro-optic effect. An interesting dimension is added when magneto-optic effects are combined with electro-optic effects in a diluted magnetic semiconductor. Diluted magnetic semiconductors (DMS's) display pronounced magneto-optic effects that can be tailored by controlling the fraction of magnetic ion, thus providing additional tunability.[5] In this paper, we present a detailed investigation of magnetophotorefractive phenomena in $Cd_{0.9}Mn_{0.1}Te$, a Mn-based II-VI DMS.[6,7] We have previously reported the demonstration of magnetophotorefractive effects using Faraday rotation.[8]

Photorefractive semiconductors are of interest for image processing applications because of their potential for high nonlinear-optical sensitivity and high speed.[9] Among the binary II-VI and III-V compound semiconductors, CdTe has the highest electro-optic coefficient r_{41} in the infrared.[10] CdTe continues to exhibit large linear electro-optic and photorefractive properties even when transition-metal ions are randomly substituted in the group-II lattice positions. The incorporation of Mn^{2+} in a II-VI semiconductor such as CdTe results in a diluted magnetic semiconductor.[6,7] A spin-spin exchange interaction couples the *d*-electron states of the Mn^{2+} ions with the *s*- and *p*-like conduction- and valence-band electrons, respectively, i.e., the so-called *sp-d* exchange interaction.[11] This exchange interaction underlies striking magneto-optic effects such as the giant Faraday and Voigt effects.[5,12,13]

Magnetophotorefractive effects rely on the Faraday rotation or on the Voigt effect during two-wave mixing. In the Faraday effect, an external magnetic field **H** induces *circular* birefringence in an otherwise optically inactive isotropic medium.[14] In addition to the Faraday rotation, the DMS's exhibit a large *linear* birefringence for light propagating at right angles to an externally applied magnetic field, i.e., the Voigt effect.[14,15]

We introduce three distinct magnetophotorefractive geometries with copropagating beams: (i) the longitudinal Faraday geometry; (ii) the transverse Faraday geometry; and (iii) the Voigt geometry. These geometries are shown in Fig. 1. In the two Faraday geometries, the optical-field polarization rotates as the beams propagate through the sample. The directions of rotation are determined by the component of the **k** vector of the optical field parallel or antiparallel to the **H** field. The Faraday geometries are not "pure" geometries, because there are components of **k** that are perpendicular to the field. These components can experience a Voigt effect. However, the Voigt effect is quadratic in magnetic field and is usually weaker than the linear Faraday effect. Therefore, in each Faraday geometry, Faraday rotation is the dom-

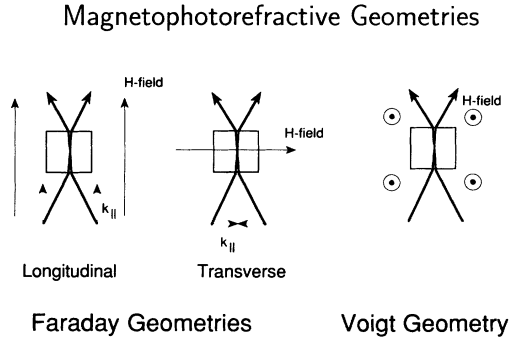

FIG. 1. The three magnetophotorefractive geometries with transmission gratings. Magnetic-field-induced circular birefringence in the Faraday geometry causes the optical-field polarizations to corotate inside the crystal in the longitudinal Faraday geometry, and to counter-rotate in the transverse Faraday geometry. Magnetic-field-induced linear birefringence in the Voigt geometry causes anisotropic photorefractive coupling.

inant magneto-optical effect. The Voigt geometry, in contrast, is a "pure" geometry because there is no component of **k** parallel to the applied **H** field. In this case, the Voigt effect introduces linear birefringence that modifies the photorefractive mixing.

II. MAGNETOPHOTOREFRACTIVE THEORY

A. Photorefractive mixing

The dependence of photorefractive two-beam coupling on crystallographic orientation was described theoretically and experimentally by Strait, Reed, and Kukhtarev for a crystal with $\bar{4}3m$ (T_d) symmetry, cut with orthogonal axes along $[1\bar{1}0]$, [110], and [001].[16] The orientations of the pump and signal laser beams relative to the coordinate axes are shown in Fig. 2. The laser beams are incident on the (110) face with symmetric incident angles, and copropagate in the y direction along the [110] axis. The angle between the $[1\bar{1}0]$ crystallographic axis and the grating vector **K** is given by ϕ. The incident polarization angles α and β for beams a and b are defined relative to the grating vector, which is parallel to the x axis.

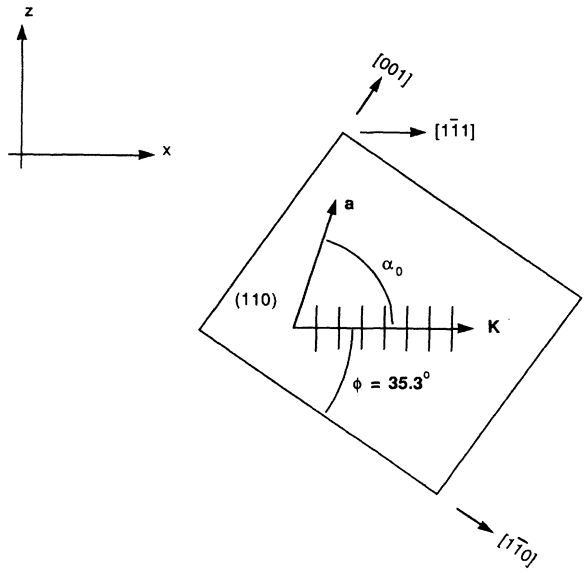

FIG. 2. For the crystal orientation and beam configuration in the two Faraday geometries, the laser beams are symmetrically incident on the (110) face and copropagate in the y direction along the [110] axis. The angle between the $[1\bar{1}0]$ crystallographic axis and the grating vector **K** along $[1\bar{1}1]$ is given by ϕ. The state of polarization is specified by angles α and β for beams **a** and **b** measured relative to the grating vector, which is parallel to the x axis.

Photorefractive two-wave mixing is a phenomena common to electro-optic crystals with extrinsic photoconductivity.[1,2] Photocarriers that are generated in bright interference fringes diffuse to dark fringes, where they are trapped by point defects. The trapped space charge is the source for an electric field that modifies the refractive index of the material through the electro-optic effect. The spatially modulated refractive index represents a diffraction grating with the same periodicity as the interference fringe pattern. The two beams that write the grating automatically satisfy the Bragg condition and diffract off the grating, with the first-order diffraction of one beam interfering constructively or destructively with the other transmitted beam. The interference produces nonreciprocal energy transfer from one beam to the other. The direction of the energy coupling is determined by the polarization of the laser beams and by the symmetry of the electro-optic tensor.

The rate of change in wave amplitude during propagation through the periodically modulated crystal is described by the coupled-wave equations in the nondepleted pump approximation. These equations for the field amplitudes **a** and **b** at near-normal incidence are[16]

$$\frac{d}{dy}\begin{bmatrix} a_x \\ a_z \end{bmatrix} = -i\frac{\pi n^3 r_{41}}{\lambda \cos\theta_{\text{in}}} E_x \begin{bmatrix} 3\cos^2(\phi)\sin(\phi) & \cos(\phi)[3\cos^2(\phi)-2] \\ \cos(\phi)[3\cos^2(\phi)-2] & \sin(\phi)[3\sin^2(\phi)-2] \end{bmatrix} \begin{bmatrix} b_x \\ b_z \end{bmatrix}, \tag{2.1}$$

where n is the refractive index, r_{41} is the nonzero electro-optic matrix element for cubic symmetry, λ is the wavelength in vacuum, and θ_{in} is the internal angle that the separate beams make with respect to the y axis. The space-charge electric field in the absence of applied electric fields is given by

$$E_x = iE_D \frac{\mathbf{a}\cdot\mathbf{b}^*}{I_a+I_b} \xi = i\xi E_D \frac{2\sqrt{I_a I_b}}{I_a+I_b}\cos(\alpha-\beta), \tag{2.2}$$

where the diffusion field is E_D. The periodic intensity distribution of the interfering beams is expressed as $I(x)=I_0[1+m\sin(Kx)]$, where $K=2\pi/\Lambda$ is the spatial frequency, $\Lambda=\lambda/2\sin\theta$ is the fringe spacing for a pump wavelength of λ, and θ is the external half-angle between the beams. The diffusion field is given by $E_D=Kk_BT/e$, where k_B is the Boltzmann constant. The wave field amplitude and intensity outside the crystal are related by $I_a=\mathbf{a}\cdot\mathbf{a}^*/2$. The factor i in Eq. (2.2) represents a shift of the diffraction grating by a quarter fringe spacing relative to the interference grating. This shift is responsible for the nonreciprocal energy transfer. The parameter ξ varies between 1 and -1 and incorporates many features of the transport and space-charge processes that are responsible for the photorefractive effect, including electron-hole competition.[17,18]

The coupled-wave equation (2.1) is sensitive to crystal orientation and beam polarization. When $\phi=35.26°$, 90°, or 144.74°, the off-diagonal matrix elements are zero, and beam coupling is isotropic. These angles correspond to the grating vector directed along the $[1\bar{1}1]$, [001], and $[\bar{1}11]$ directions. On the other hand, for $\phi=0°$ the grat-

ing vector is oriented along $[1\bar{1}0]$, and the diagonal elements are zero. These special crystal orientations can be used to advantage during experiments by allowing only one magneto-optic effect at a time to modify the photorefractive beam coupling.

In the theoretical discussion of the magnetophotorefractive geometries, we make several simplifying assumptions. First, we neglect all influence of magnetotransport effects on photorefractive mixing. Second, the magnetic permeability is assumed to be a constant. Third, we neglect magnetic-field-induced dichroism, which causes different absorption for different polarizations.[19,20] Magnetotransport effects can be important during photorefractive mixing for special circumstances[21] under large applied electric and magnetic fields. We use no applied electric fields in our experiments, for which the magnetotransport effects do not influence wave mixing. On the other hand, we cannot rule out the effect of magnetic dichroism in our experiments above 10 kG for photon energies close to the band gap or for high magnetic fields. Therefore our theoretical discussion is limited to small-field effects. High-field effects will be considered in a later paper.

B. Faraday photorefractive geometries

In a longitudinal magnetic field, the eigenmodes of propagation are σ_+ and σ_- circularly polarized light,

$$\hat{\sigma}_\pm=\frac{1}{\sqrt{2}}\begin{bmatrix}1\\ \pm i\end{bmatrix}.$$

For photon energies slightly smaller than the interband transition, the refractive index is dominated by the interband $\Gamma_8-\Gamma_6$ transition.[12] The magnetic field splits the spin degeneracy of the transition, shifting the transition energies differently for the different helicities. The σ_+ and σ_- circular polarization refractive indices can be expressed as

$$n_+=n_0-\Delta n(H),\quad n_-=n_0+\Delta n(H),$$

where n_0 is approximately independent of magnetic field, and $\Delta n(H)$ is approximately linear with H, for small fields. The Faraday rotation angle, at a distance y inside the sample, is given by

$$\Theta_F(y)=\Delta n k y=V(\hat{\mathbf{k}}\cdot\mathbf{H})y,$$

where V is the Verdet constant in units of degree/G cm, and $\hat{\mathbf{k}}$ is the unit $\mathbf{k}$ vector. For the incident $\mathbf{b}$ beam linearly polarized at an angle β_0 with respect to the x axis, the electric-field vector at y inside the crystal is given by

$$\begin{aligned}\mathbf{b}(y)&=\frac{b_0}{2}\left\{e^{\text{in}_-ky}\begin{bmatrix}1\\ i\end{bmatrix}e^{i\beta_0}+e^{\text{in}_+ky}\begin{bmatrix}1\\ -i\end{bmatrix}e^{-i\beta_0}\right\}\\&=b_0e^{\text{in}_0ky}\begin{bmatrix}\cos(\beta_0+\Theta_F^b(y))\\ \sin(\beta_0+\Theta_F^b(y))\end{bmatrix}.\end{aligned}\tag{2.3}$$

The expression for the $\mathbf{a}$ beam is obtained by replacing β_0 in Eq. (2.3) by α_0, and b by a.

In our analysis of the magnetophotorefractive effect we choose to represent the problem in terms of a fixed external reference frame within which Eq. (2.1) for linear polarizations is used at each position y along the beam direction. The increment $d\mathbf{a}(y)$ at y depends on the local orientations of $\mathbf{a}(y)$ and $\mathbf{b}(y)$ at y. The contribution of $d\mathbf{a}(y)$ must propagate from y to L, during which the polarization experiences additional rotation. The output polarization state of $d\mathbf{a}(y)$ must therefore be included as the increments are integrated over the length of the crystal.

For linearly polarized beams in the presence of a longitudinal magnetic field directed along the y axis, the coupled-wave equations Eq. (2.1) at a distance y inside the crystal become

$$\frac{d}{dy}\begin{bmatrix}a_x\\ a_z\end{bmatrix}=-i\frac{\pi n^3 r_{41}}{\lambda\cos\theta_{\text{in}}}E_x\begin{bmatrix}3\cos^2(\phi)\sin(\phi) & \cos(\phi)[3\cos^2(\phi)-2]\\ \cos(\phi)[3\cos^2(\phi)-2] & \sin(\phi)[3\sin^2(\phi)-2]\end{bmatrix}\begin{bmatrix}\cos[\beta_0+\Theta_F^b(y)]\\ \sin[\beta_0+\Theta_F^b(y)]\end{bmatrix}b_0.\tag{2.4}$$

To find the x and y components at the exit face, the incremented electric-field vector components at y must propagate from y to L with the appropriate rotation. The incremented output field $d\mathbf{a}(y;L)$ is given by

$$\begin{aligned}\frac{d\mathbf{a}(y;L)}{dy}=&-i\frac{\pi n^3 r_{41}}{\lambda\cos\theta_{\text{in}}}E_x\begin{bmatrix}\cos[\Theta_F^a(L-y)] & \sin[\Theta_F^a(L-y)]\\ -\sin[\Theta_F^a(L-y)] & \cos[\Theta_F^a(L-y)]\end{bmatrix}\\&\times\begin{bmatrix}3\cos^2(\phi)\sin(\phi) & \cos(\phi)[3\cos^2(\phi)-2]\\ \cos(\phi)[3\cos^2(\phi)-2] & \sin(\phi)[3\sin^2(\phi)-2]\end{bmatrix}\begin{bmatrix}\cos[\beta_0+\Theta_F^b(y)]\\ \sin[\beta_0+\Theta_F^b(y)]\end{bmatrix}b_0\end{aligned}\tag{2.5}$$

because the incremented electric-field vector $\mathbf{a}$ experiences additional Faraday rotation as it propagates from y to the back of the crystal at L.

The intensity of the probe beam is measured at the exit face of the photorefractive crystal. In this discussion, we follow the formalism of Ref. 16 and view the output intensity of beam $\mathbf{a}$ through a linear analyzer oriented along the x or the z axes. The change in x and z components of beam $\mathbf{a}$ at the exit face are given by

$$\Delta I_{ax}(L)=\frac{1}{2}\left|a_0\cos[\alpha_0+\Theta_F^a(L)]+\int_0^L\frac{da_x(y;L)}{dy}dy\right|^2-\tfrac{1}{2}|a_0\cos[\alpha_0+\Theta_F^a(L)]|^2\ ,$$
$$\Delta I_{az}(L)=\frac{1}{2}\left|a_0\sin[\alpha_0+\Theta_F^a(L)]+\int_0^L\frac{da_z(y;L)}{dy}dy\right|^2-\tfrac{1}{2}|a_0\sin[\alpha_0+\Theta_F^a(L)]|^2\ , \tag{2.6}$$

where the first term on the right-hand side gives the total intensity of the probe beam at the output with coherent interference between the direct beam and the increment from the beam coupling. The second terms in the respective equations are the beam intensities in the absence of coupling. The photorefractive gain Γ for small modulation is given by

$$\Gamma=\frac{1}{L}\ln\left[\frac{\Delta I_{ax}(L)+\Delta I_{az}(L)}{I_{ax}(L)+I_{az}(L)}+1\right]. \tag{2.7}$$

In the following sections, we describe the longitudinal and transverse Faraday geometries. For both Faraday geometries, the grating vector is oriented parallel to a $\langle 111\rangle$ axis with $\phi=35.3°$ shown in Fig. 2. This orientation gives the largest photorefractive gain[16] and produces large Faraday photorefractive effects.[8] The Voigt effect makes no contribution to photorefractive two-wave mixing for this orientation.

1. Longitudinal Faraday geometry

In the longitudinal Faraday geometry, shown in Fig. 1(a), the **a** and **b** beams copropagate in the direction of the applied magnetic field. Because the internal angle θ_{in} is small, the **k** vectors are directed nearly parallel to the magnetic field, with only a small component of the **k** vector normal to the field. For linearly polarized beams, this geometry produces Faraday rotation in each beam, causing the polarization vectors to corotate during propagation through the crystal.

The results of Eqs. (2.5)–(2.7) for the longitudinal geometry are shown in Fig. 3 for $\alpha_0=\beta_0$ for fixed initial p and s polarizations as functions of magnetic field. The magnetic field changes the sign of the gain in the s-polarized case. The photorefractive gains for both polarizations oscillate with increasing field, undergoing one oscillation for each 180° of Faraday rotation. The oscillations are damped as the gain approaches an average value for large rotations. The high-field gain in Fig. 3 represents a running average for multiple rotations, with the orientational dependences averaged out.

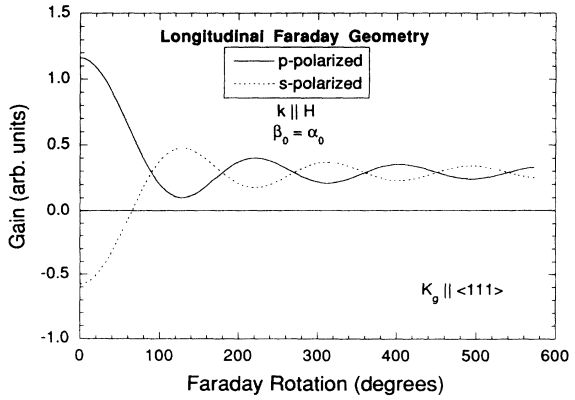

FIG. 3. Calculated photorefractive gain for the longitudinal Faraday geometry as a function of applied magnetic field with $\phi=35.3°$ and the grating vector parallel to the $[1\bar{1}1]$ axis. The initial polarization conditions are s and p polarized. The gain approaches its average value for high magnetic fields.

2. Transverse Faraday geometry

The transverse Faraday geometry in Fig. 1(b) differs in two important aspects from the longitudinal geometry in Fig. 1(a). First, the two beam polarizations counter-rotate because the **k** vectors of the copropagating beams have equal but opposite components in the direction of the applied magnetic field:

$$\hat{\mathbf{k}}_a\cdot\mathbf{H}=-\hat{\mathbf{k}}_b\cdot\mathbf{H}\ ,$$
$$\Theta_F^a=-\Theta_F^b\ .$$

The counter-rotation produces a behavior significantly different for the transverse geometry from that for the longitudinal. One of the most dramatic differences is the finite beam coupling for initially orthogonally polarized beams. The second aspect is that much larger magnetic fields must be applied to produce significant Faraday rotations because of the small $\mathbf{k}_\parallel$-component in the crystal.

The magnetophotorefractive equations for the transverse Faraday geometry are also given by Eqs. (2.5)–(2.7). Equation (2.2) is replaced by

$$E_x(y)=i\xi E_D\frac{2\sqrt{I_aI_b}}{I_a+I_b}\cos[\alpha_0-\beta_0+\Theta_F^a(y)-\Theta_F^b(y)]\ , \tag{2.8}$$

accounting for the change in the space-charge field with distance y into the crystal caused by the counter-rotating beams.

Two initial polarization cases were simulated for the transverse Faraday geometry: (1) equal initial polarizations $\alpha_0=\beta_0$; and (2) orthogonal initial polarizations $\beta_0=\alpha_0+90°$. The magnetic-field dependences are shown in Fig. 4. The values for photorefractive gain for equal initial beam polarizations shown in Fig. 4(a) approach a different average value compared to the longitudinal case for large rotations. The second case with orthogonal initial polarizations shown in Fig. 4(b) exhibits qualitatively different behavior, because in the absence of a magnetic field this initial polarization condition produces zero photorefractive gain for all polarization angles. With increasing magnetic field, the counter-rotation of the polarization vectors causes finite coupling.

C. Voigt geometry

In the Voigt geometry, shown in Fig. 1(c), the **a** and **b** beams copropagate along the y axis perpendicular to the magnetic field applied along the z axis. The Voigt effect is a magnetic-field-induced linear birefringence. For linearly polarized light, the component of the electric-field vector parallel to the magnetic field experiences a different refractive index than the electric-field vector perpendicular to the magnetic field. It has been shown that, close to the energy gap of a DMS, the Zeeman splitting of the excitonic transitions governs both the Faraday and Voigt effects. Further, the $\sigma_{\pm}$ transitions underlie the Faraday effect, whereas both $\sigma_{\pm}$ and p transitions come into play in the Voigt effect.[12,13,20] The refractive indices for the parallel and perpendicular polarizations can be expressed as

$$n_{\parallel}=n_0+\Delta n_{\parallel}(H),\quad n_{\perp}=n_0+\Delta n_{\perp}(H)\ ,$$

where n_0 is approximately independent of magnetic field and $\Delta n(H)$ is approximately a quadratic function of the magnetic field, for small fields. By analogy with the Faraday effect the phase angle between the orthogonal polarizations is given by

$$\Theta_V(y)=(\Delta n_{\perp}-\Delta n_{\parallel})ky=Y|(\hat{\mathbf{k}}\times\mathbf{H})|^2y\ ,$$

where Y is the Voigt analog to the Verdet constant.

The coupled-wave equations describing the increment in the field vector of the **a** beam at the output of the crystal are

$$\frac{d\mathbf{a}(y;L)}{dy}=-i\frac{\pi n^3 r_{41}}{\lambda\cos\theta_{\text{in}}}E_x\begin{bmatrix}\exp(i\Delta n_{\parallel}k(L-y)) & 0\\ 0 & \exp[i\Delta n_{\perp}k(L-y)]\end{bmatrix}\times\begin{bmatrix}3\cos^2(\phi)\sin(\phi) & \cos(\phi)[3\cos^2(\phi)-2]\\ \cos(\phi)[3\cos^2(\phi)-2] & \sin(\phi)[3\sin^2(\phi)-2]\end{bmatrix}\begin{bmatrix}\exp(i\Delta n_{\parallel}ky)\cos(\beta_0)\\ \exp(i\Delta n_{\perp}ky)\sin(\beta_0)\end{bmatrix}b_0\ . \tag{2.9}$$

The intensities observed through x- and z-oriented analyzers are

$$\Delta I_{ax}(L)=\frac{1}{2}\left|a_0\exp(i\Delta n_{\parallel}kL)\cos(\alpha_0)+\int_0^L\frac{da_x(y;L)}{dy}dy\right|^2-\tfrac{1}{2}|a_0\exp(i\Delta n_{\parallel}kL)\cos(\alpha_0)|^2\ , \tag{2.10}$$

$$\Delta I_{az}(L)=\frac{1}{2}\left|a_0\exp(i\Delta n_{\perp}kL)\sin(\alpha_0)+\int_0^L\frac{da_z(y;L)}{dy}dy\right|^2-\tfrac{1}{2}|a_0\exp(i\Delta n_{\perp}kL)\sin(\alpha_0)|^2\ ,$$

and the gain is still given by Eq. (2.7).

For the Voigt photorefractive experiments, the photorefractive coupling must not be isotropic. When the photorefractive coupling is isotropic [i.e., when the off-diagonal matrix elements in Eq. (2.4) are zero] there is no coupling between the polarizations parallel and perpendicular to the applied magnetic field. Therefore in the Voigt experiments we choose $\phi=0°$ in order to observe the Voigt-photorefractive effect. For $\phi=35.26°$, 90°, or 144.74° the Voigt effect, although possibly strong, would not alter the photorefractive mixing. The mixing in the presence of the Voigt effect is shown in Fig. 5, plotted as a function of H^2 for $\phi=0°$ with the grating vector parallel to a $\langle 110\rangle$ axis. A Voigt phase shift of 180° between the vertical and horizontal polarizations make the gain vanish for all polarizations.

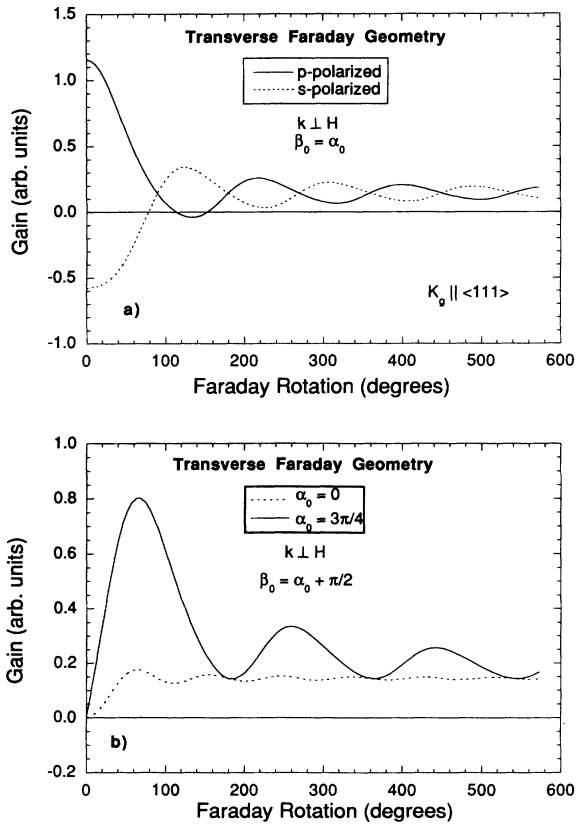

FIG. 4. Calculated photorefractive gain for the transverse Faraday geometry as a function of magnetic field with $\phi=35.3°$ and the grating vector parallel to the $[1\bar{1}1]$ axis. Four initial polarization conditions are shown. For equal initial polarizations $\beta_0=\alpha_0$, in Fig. (a) the incident polarization conditions are s and p polarized. Results are also shown in (b) for cross-polarized conditions $\beta_0=\alpha_0+90°$.

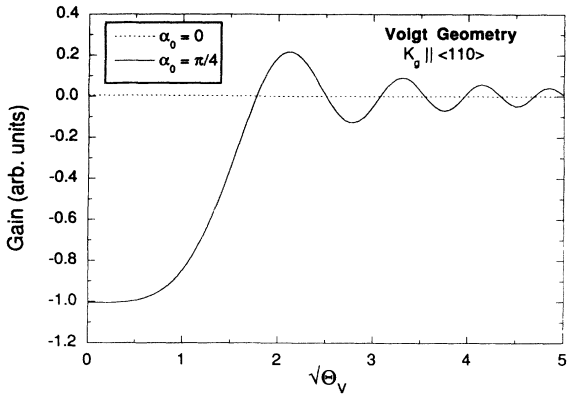

FIG. 5. Calculated two-wave mixing gain as a function of $\sqrt{\Theta_v}$ in the Voigt geometry for $\phi=0°$ with the grating vector parallel to the $[1\bar{1}0]$ axis. The gain changes sign at $\Theta_v=180°$ with $\alpha_0=45°$, and oscillates with decreasing amplitude about zero value for higher magnetic fields.

III. EXPERIMENTAL RESULTS

A. Photorefractive characterization

1. Experiment

In our studies of the magnetophotorefractive effect, we used a nominally undoped crystal of modified-Bridgeman-growth $Cd_{0.9}Mn_{0.1}Te$. After growth, the crystal was oriented by x-ray diffraction and cut into a parallelepiped with edges along [110], $[1\bar{1}0]$, and [001]. The sample length in the direction of propagation in the experiments along [110] was 0.79 cm. In all our experiments, the fringe spacing Λ was approximately 4 μm.

In the two-wave mixing experiment, the laser beam from a Kr^+ laser, operating in fundamental transverse mode (TEM_{00}), with an emission wavelength of 799 nm is split by a beam splitter into a pump beam and a signal beam. The signal beam is made weaker to work in the small-amplitude-modulation approximation ($m \ll 1$). The two beams are directed onto the sample, mounted inside a Janis variable-temperature superconducting magnet cryostat. We measured the two-wave mixing gain by mechanically chopping the pump beam and measuring the modulation of the probe beam intensity using a Si photodiode and a lock-in amplifier.

The incident polarization is controlled using half-wave plates after the beam splitter in both the pump and the probe beams. The two plates allow an accurate determination of the input polarization of the two beams and remove systematic misalignment caused by imperfection in the beam splitter. The Faraday rotation is measured for both the pump and the probe beam by placing an analyzer after the sample and monitoring the transmitted intensity. All the polarizations are accurate within 2°–3°.

The photorefractive properties of the sample were first characterized by performing two-wave mixing at 1.06 μm using an yttrium aluminum garnet (YAG:Nd) laser. A laser intensity of ~ 1 W/cm^2 was necessary to saturate the photorefractive gain at room temperature because of the small dark resistivity of 10^6 Ω cm. When the sample was cooled to 220 K the dark resistivity increased by two orders of magnitude to approximately 10^8 Ω *cm*, and much smaller laser intensities could be used to saturate the gain. Near 220 K, photorefractive gains approaching 0.1 cm^{-1} were observed for a fringe spacing of 3.8 μm, with a pump-to-probe beam intensity ratio of 1000:1. The magnetophotorefractive gain measurements were done at 220 K for reasons explained below.

2. Temperature dependence of photorefractive effect

The photorefractive effect is useful not only for optical imaging applications, but also works as a probe of material properties, performing as a deep-level defect spectroscopy[22–24] which can be used to study nonequilibrium charge-state occupancies of defects.[25–27] The photorefractive effect depends explicitly on charge trapped at defects within the material. Therefore the type of defects, their concentrations, binding energies, and optical cross sections can strongly influence photorefractive beam coupling. By studying the two-wave mixing gain as a function of temperature, the contribution of different defect species to the photorefractive behavior can be determined.

The temperature dependence of two-wave mixing gain in $Cd_{0.9}Mn_{0.1}Te$ at 799 nm was measured with the crystal orientation shown in Fig. 2, corresponding to $\phi=35.3°$ with the grating vector (**K**) along $[1\bar{1}1]$. The temperature dependence is shown in Fig. 6. The fringe spacing was 4 μm, with a pump-to-probe intensity ratio of 700:1. The optical fields were *p* polarized (parallel to the plane of incidence) to work with maximum gain for this crystal orientation.[16] The gain exhibits a nonlinear temperature dependence. The striking feature is the change in the sign of the gain near 100 K, signifying a change in the direction of energy transfer. The direction of energy transfer is determined by the crystallographic orientation of the crystal (the sign of the electro-optic coefficient), and by the sign of the dominant photocarriers. The observed temperature behavior is in sharp contrast to the linear temperature dependence predicted by the single-

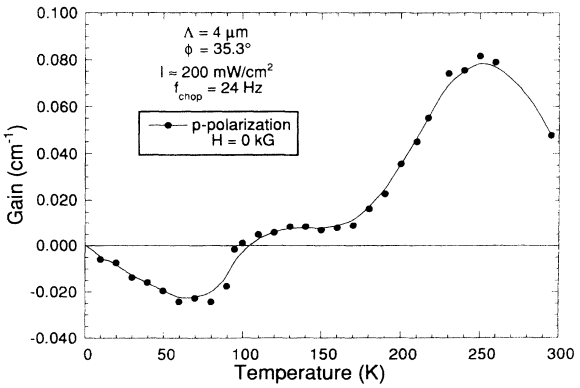

FIG. 6. Temperature dependence of two-wave mixing gain for *p* polarization of the optical fields. The change in the sign of gain near 100 K indicates a change in the sign of dominant photocarriers and a change in the direction of the energy transfer. The solid line is to guide the eye.

defect model of the photorefractive effect. This behavior can be explained by including the effects of additional defect levels in the crystal.[24,25] Note that the gain achieves its maximum value near 250 K, with a sharp drop off below it. To work with large gains, we choose the temperature of the sample to be 220 K. This temperature is also optimum to produce large magneto-optic effects, as explained in Sec. III B 3.

3. *Temperature dependence of magneto-optic effects*

In addition to controlling defect charge states, temperature also determines the strengths of the magneto-optic effects in diluted magnetic semiconductors. The Faraday rotation depends on the Verdet constant $V(x,\lambda,T)$, which is proportional to magnetization M, and is a function of the magnetic ion (Mn^{2+}) concentration x and the temperature T of the sample. The magnetization and the Verdet constant increase as temperature decreases, allowing larger Faraday rotation at smaller applied magnetic-field strengths. $Cd_{1-x}Mn_xTe$ can be grown as a single crystal up to $x=0.77$ in the bulk,[7] although the value of x for maximum magnetization depends on temperature. For instance, at room temperature M increases with increasing x, whereas at low temperatures the antiferromagnetic coupling between Mn^{2+} ions can cause M to decrease with increasing x. The wavelength dependence of the Verdet constant is such that it is resonantly enhanced for photon energies close to the band edge. Therefore, we use a photon energy of 1.55 eV corresponding to the 799-nm line of the Kr^+ laser, which is close to the band-gap energy 1.69 eV of $Cd_{0.9}Mn_{0.1}Te$ at 220 K.

In the Voigt effect, the phase difference between the components parallel and perpendicular to the magnetic field, called the Voigt phase shift, depends on the square of the magnetization with the proportionality factor $Y(x,\lambda,T)$. The dependence on T and x is more pronounced than in the Faraday effect. The Voigt effect is also enhanced for photon energies close to the band gap, as for the Faraday effect.[13]

B. Magnetophotorefractive geometries

1. *Longitudinal Faraday geometry*

The sample orientation, the grating vector **K**, and the polarization of the optical fields for the Faraday geometries, are shown in Fig. 2. This orientation, corresponding to $\phi=35.3°$, is chosen for three reasons. First, in the absence of an applied dc magnetic field, p-polarized incident beams achieve the largest photorefractive gain with this orientation.[16] Second, the gain changes sign as the incident-beam polarization is changed between s and p-polarizations. Third, there is no Voigt-photorefractive effect for this crystal orientation because the coupling is isotropic. All the data for the Faraday geometries were taken at $T=220$ K. This temperature was chosen to improve both the dark resistivity and the magneto-optic effects. The assignment of positive and negative directions to the magnetic field is arbitrary.

In this configuration, the direction of propagation of the laser beams is approximately parallel to the applied dc magnetic field. The magnetic field rotates the polarization angle α within the sample according to $\alpha(y)=\alpha_0+\Theta_F$, with both beams undergoing the same rotation in the same direction (corotating). The Verdet constant for our sample is $V=0.076$ (deg/G cm) at 220 K for 799 nm. A modest field of 1.5 kG is therefore sufficient to produce a 90° Faraday rotation as the beam traverses the entire 0.79-cm length of the crystal.

The gain as a function of the incident polarization is shown in Fig. 7 for applied dc magnetic fields of 0, +1.5, and −1.5 kG. The polarization angle $\alpha_0=90°$ corresponds to incident s polarization (perpendicular to the incident plane), and $\alpha_0=0°$ and 180° corresponds to incident p polarization (parallel to the incident plane). The zero-field data provide the reference for interpreting the magnetic-field data. In the *presence* of an applied dc magnetic field, the gain is determined by averaging $\Gamma(\alpha)$ over zero-field values from the initial polarization state $\alpha=\alpha_0$ to the final polarization state $\alpha=\alpha_0+\Theta_F$. This produces a shift in the gain curve peak position and a reduction in its magnitude. For example, for $H=+1.5$ kG (corresponding to $\Theta_F=90°$) with $\alpha_0=0°$, the magnitude of the gain is determined by averaging the zero-field Γ from $\alpha_0=0°$ to $\alpha_0=90°$. Similarly the gain curve maximum for $H=+1.5$ kG occurs at $\alpha_0=45°$ and has a value ~ 0.04 cm^{-1}, corresponding to the zero-field value of $\Gamma(\alpha)$ averaged over α_0 from +45° to −45°. The gain for $H=-1.5$ kG has the opposite sign relative to $H=+1.5$ kG because the rotation of the optical-field polarization is in the opposite sense. The solid curves in Fig. 7 are fits from the theory of Eqs. (2.5)–(2.7).

The experimental two-wave mixing behavior in Fig. 7 qualitatively agrees with the simulations. However, the experimental data include a constant offset. This additional contribution to the two-wave mixing arises from induced absorption gratings, which has not been included in the theoretical formulation described in Sec. II. In photorefractive crystals absorption gratings appear in addition to electro-optic gratings[28–34] because the space

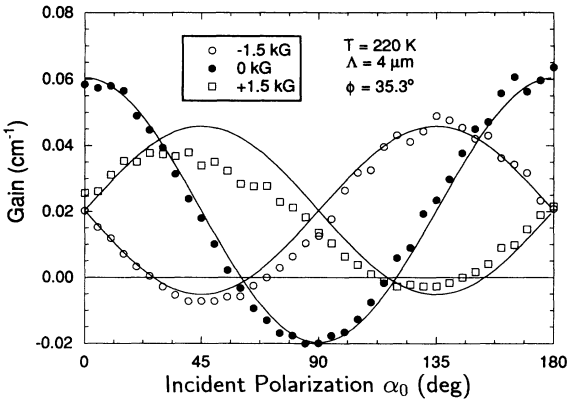

FIG. 7. Experimental two-wave mixing gain as a function of incident polarization of optical fields in the longitudinal Faraday geometry for $H=0$, 1.5, and −1.5 kG. The data at $H=\pm 1.5$ kG correspond to a ±90° Faraday rotation through the sample. The solid lines are a fit to the theory with a contribution from absorption gratings.

charge trapped at deep defects (which generates the space-charge electric fields) also changes the absorption by defect photoionization. The coupling from absorption gratings is insensitive to the state of polarization of the incident optical fields. The contribution from the absorption grating in Fig. 7 is $\Delta\alpha \approx 0.007\ \mathrm{cm}^{-1}$.

Two-beam coupling modulation as a function of a dc magnetic field is demonstrated in Fig. 8 for incident p and s polarizations. The direction of energy transfer for s polarization can be reversed by applying a modest magnetic field of 1 kG. The oscillatory behavior of gain about its average value with increasing magnetic field can be understood in terms of the averaging process described above. The magnetic oscillation period is determined by the optical path length and the Verdet constant. Increasing either the crystal length or the Verdet constant (e.g., by decreasing the temperature or increasing the Mn fraction) increases the total Faraday rotation and decreases the magnetic oscillation period.

Under the given experimental conditions, ideally we would expect the gain for the incident p polarization to cross the average line (shown by a dotted line) at increments of 1.5 kG, corresponding to successive Faraday rotations of 90°. This behavior was shown in the simulation in Fig. 3. The experimental gain agrees qualitatively with the simulation only up to 3 kG, with crossings occurring approximately at 1.5 and 3 kG. However, there is significant deviation from the simulation for large magnetic-field strengths. This behavior of gain for higher magnetic fields is not currently understood, and will be the focus of future work.

2. *Transverse Faraday geometry*

In this geometry the magnetic field is applied normal to the direction of propagation of the laser beams, as shown in Fig. 1(b). Because the angle between **H** and **k** is not exactly 90°, there is a component of magnetic field $H_{\parallel} = H\sin\theta$ parallel to **k** and a component $H_{\perp} = H\cos\theta$ perpendicular to **k**, where θ is te half-angle inside the crystal. Even though $H_{\perp}$ is much larger than $H_{\parallel}$, the dominant magneto-optic effect is the Faraday rotation.

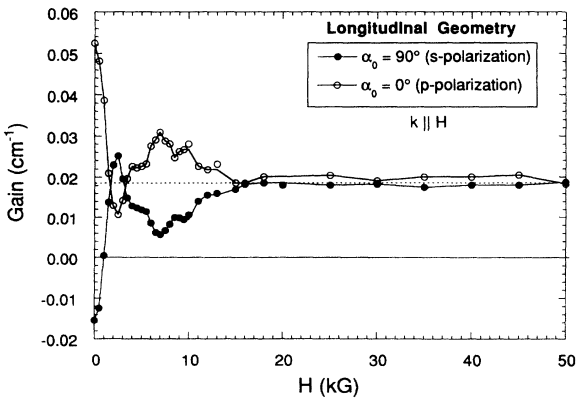

FIG. 8. Experimental gain for s and p polarizations in the longitudinal Faraday geometry as a function of magnetic field. Above 3 kG the behavior deviates significantly from the predictions of Fig. 3. The solid lines are to guide the eye.

The perpendicular component of the magnetic field $H_{\perp}$ for the crystal orientation in Fig. 2 will not induce a Voigt photorefractive effect because the coupling is isotropic for this orientation. However, much larger magnetic fields are needed to produce a given Faraday rotation, because of the small value of the angle θ.

In the transverse geometry, both optical fields will undergo the same polarization rotation, but in the opposite directions (counter-rotating) inside the crystal. The angle of polarization rotation is given by $\alpha(y) = \alpha_0 + VH_{\parallel}y$ and $\beta(y) = \beta_0 - VH_{\parallel}y$ for the two laser beams, where α_0 and β_0 are the incident polarizations at $y = 0$. Experimental results are presented here when the initial polarizations are prepared according to the following two different cases: (i) equal initial polarizations $\beta_0 = \alpha_0$, and (ii) orthogonal initial polarizations $\beta_0 = \alpha_0 + 90°$. The gain as a function of incident polarization for case (i) is shown in Fig. 9 for fixed magnetic fields of $H = 0$, $+23.6$ kG, and ± 47.2 kG, corresponding to Faraday rotations of 0°, 45°, and ±90°, respectively. The results for case (ii) are shown in Fig. 10. The solid curves are the fit from the theory of Eqs. (2.5), (2.6), and (2.8) using the same fitting parameters as in Fig. 7.

There are two important features of the gain curves in Fig. 9. First, the average gain is 0.01 cm^{-1}, which is smaller than the average gain for the corresponding case in the longitudinal geometry. Second, the gain in the transverse geometry is insensitive to the direction of the applied magnetic field because the polarization rotation is symmetric with respect to the direction of the applied magnetic field (see the curves for $H = \pm 47.2$ kG).

The behavior of photorefractive gain as a function of magnetic field is shown in Fig. 11 for both initial polarization cases. Here the incident polarization of both beams is fixed, and the magnetic field is varied. For the initial p and s polarizations, the two-wave mixing gain oscillates about its average value as a function of applied magnetic field. This behavior is qualitatively similar to

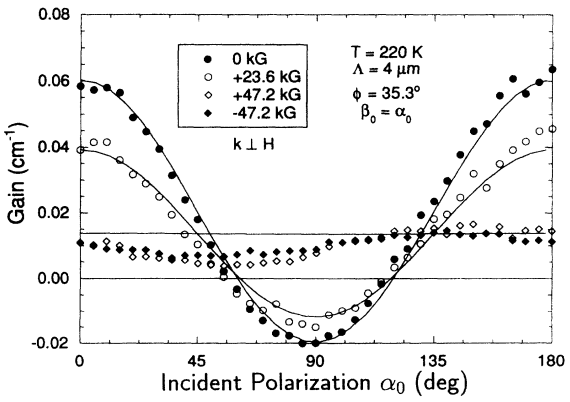

FIG. 9. Experimental two-wave mixing gain as a function of incident polarization in the transverse Faraday geometry for fields of $H = 0$, 23.6, and ± 47.2 kG representing fixed Faraday rotations of $\Theta_F = 0°$, $+45°$, and $\pm 90°$. Much larger magnetic fields are needed to produce a given Faraday rotation compared with the longitudinal case. The solid curves are the fit from the theory.

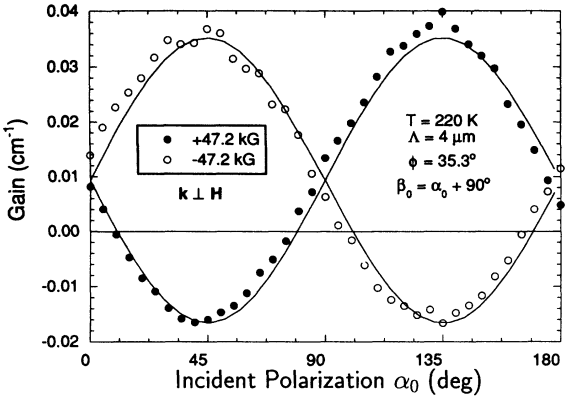

FIG. 10. Experimental two-wave mixing gain as a function of incident polarization in the transverse Faraday geometry for fields of $H = \pm 47.2$ kG representing fixed Faraday rotations of $\Theta_F = \pm 90°$. The solid curves are the fit from the theory.

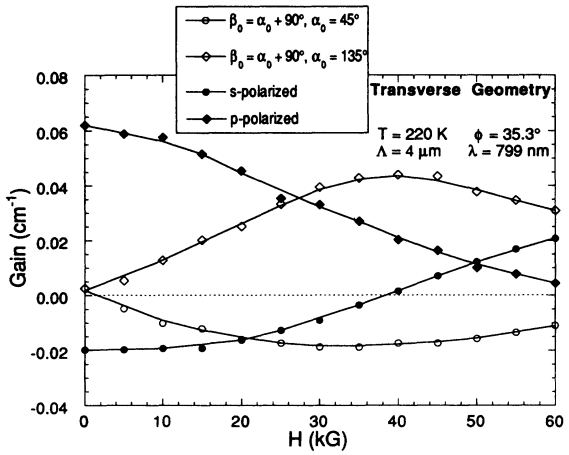

FIG. 11. Experimental gain as a function of magnetic field for the transverse Faraday geometry using parallel s and p polarizations, and cross polarization. The solid lines are to guide the eye.

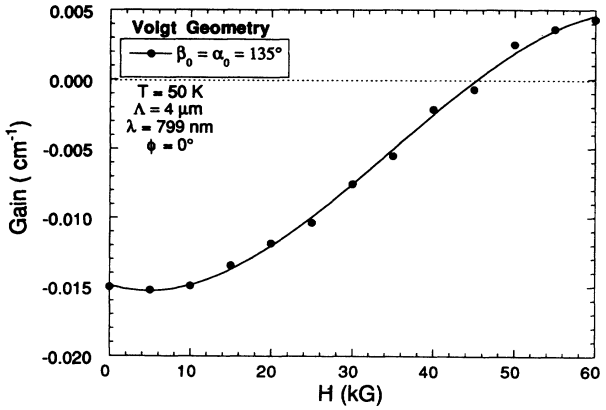

FIG. 12. Experimental gain as a function of applied magnetic field in the Voigt geometry. The beams are propagating along [110], with the grating vector along [1$\bar{1}$0] and the magnetic field applied along [001]. The data are qualitatively in agreement with the simulations in Fig. 5. Note the change in the sign of gain at $H \approx 45$ kG. The solid line is to guide the eye.

the gain behavior in the longitudinal geometry. Quantitatively, however, there are two important differences. First, the period of oscillations is much larger; and second, the gain approaches a lower average value for large magnetic fields. For the orthogonal initial polarization case (ii) we used $\alpha_0 = 45°$ and 135°. Note that in the absence of an applied magnetic field, there is no coupling between two orthogonally polarized optical fields and therefore the gain is zero. However, as the magnetic field is applied, the two fields begin to couple because of the change in their polarization states inside the sample. This feature of the gain behavior makes the transverse geometry distinct from the longitudinal geometry, and can be used to turn on/off the photorefractive coupling by turning on/off the external magnetic field.

3. *Voigt geometry*

To characterize the Voigt effect, we first measured the Voigt phase shift by increasing the magnetic field from 0 to 60 kG. The incident beam was polarized at 45° with respect to **H**, and was analyzed with a linear polarizer at −45° after transmission through the sample. In this configuration the transmitted intensity varies as $\sin^2(\theta_v/2)$ and exhibits maxima at $\Theta_v = (2p+1)\pi$ and minima at $\Phi_v = 2p\pi$, where p is an integer. The transmission curve was used to calculate the Voigt phase shift. A deviation from linearity at high fields, above approximately 30 kG, was observed due to the saturation of magnetization.[13] This saturation is more pronounced for low Mn concentrations, low temperature, and high fields.

To study the beam coupling in the presence of the Voigt effect, the crystal orientation was changed from $\phi = 35.5°$ to $\phi = 0°$, so that the beam coupling was no longer isotropic. The laser beams propagated along [110] with the magnetic field applied along [001], and the grating vector parallel to [1$\bar{1}$0] with a grating spacing of 4 μm. To increase the Voigt effect the temperature was further lowered to 50 K. The incident polarization for both the pump and the probe laser beams was 135°, which made an angle of 45° with respect to the magnetic-field-induced optic axis. In order to minimize the effect of the polarization change from the cryostat windows at this lower temperature, a linear polarizer was mounted at 135° onto the front face of the crystal *inside* the cryostat. The measured gain as a function of the applied magnetic field is shown in Fig. 12, which is qualitatively in agreement with the simulations in Fig. 5. The gain changes sign, signifying a change in the direction of energy transfer at about 45 kG, which corresponds to a Voigt phase shift of approximately 100°.

IV. DISCUSSION

In our study of magnetophotorefractive effects in unintentionally doped $Cd_{0.9}Mn_{0.1}Te$, we purposely avoided discussion of the point defects that are responsible for the weak semi-insulating behavior of our crystal and for the trapped space-charge gratings that lead to the photorefractive effect. Deep defects in the diluted magnetic semiconductors have not been studied extensively, al-

though there is considerably evidence that self-compensation by point defects in II-VI semiconductors is common. Because of the relatively low resistivity at room temperature, and the rapid increase of the resistivity by two orders of magnitude when the temperature was reduced to 220 K, we can conclude that the Fermi level in our crystal is pinned by a relatively shallow "deep" defect level. The change in the sign of the gain below 100 K is evidence that an additional and even shallower defect level is also present in this material. Because of the central role that deep defects play in the photorefractive effect, it will be necessary to understand and control the defects states in diluted magnetic semiconductors in future magnetophotorefractive studies.

In order to enhance the Faraday and Voigt magneto-optic effects, our experiments were performed with a laser photon energy tuned close to the interband transition energy. The magneto-optics for this laser energy is dominated by excitonic effects. Such excitonic enhancement can also play an important role in enhanced electro-optic effects. The electroabsorption near the fundamental band gap is the source of quadratic electro-optic effects that can significantly enhance photorefractive gratings[35,36] when electric fields are applied. Combining enhanced magneto-optics with enhanced excitonic electro-optics is an area for future work in magnetophotorefractive effects. In addition, working with near-resonant excitation of the semiconductor and/or with electric fields should lead to interesting physical aspects, including magnetic-field-induced dichroism and magneto-transport effects.

Several outstanding issues remain in our study of magnetophotorefractive effects. Most notably, the behavior of the photorefractive coupling for large Faraday rotations does not agree with the model presented in this paper. A more detailed model of the beam coupling should include transport effects as well as circular dichroism. Finally, reflection geometries with counterpropagating light beams are an important class of geometries yet to be explored. The reflection geometries lead to four-wave mixing and, most importantly, phase conjugation, which is one of the most commonly studied and important photorefractive effects with many potential applications. Phase conjugation can be described as time reversal of light, and is possible in materials with time-reversal symmetry. Because magnetic fields remove time-reversal degeneracy, magnetophotorefractive effects will provide a way to control and quench phase conjugation.

ACKNOWLEDGMENTS

R.S.R. thanks G. A. Sefler for helpful discussions. D.D.N. acknowledges support by the Presidential Young Investigator Program in the Division of Materials Research of NSF, and by the Alfred P. Sloan Foundation. A.K.R. acknowledges support by a grant from the National Science Foundation (Materials Research Group Grant No. DMR92-21390).

*Electronic address: Internet: rana@physics.purdue.edu

[1]P. Yeh, *Introduction to Photorefractive Nonlinear Optics,* (Wiley, New York, 1993).
[2]P. Gunter and J. P. Huignard, *Topics of Applied Physics, Photorefractive Materials and Their Applications,* (Springer-Verlag, Berlin, 1989), Vols. 61 and 62.
[3]D. L. Staebler and J. J. Amodei, J. Appl. Phys. **43**, 1042 (1972).
[4]N. Kukhtarev, V. Markov, S. Odulov, M. Soskin, and V. Vinetskii, Ferroelectrics **22**, 949 (1979).
[5]J. A. Gaj, R. R. Galazka, and M. Nawrocki, Solid State Commun. **25**, 193 (1978).
[6]*Diluted Magnetic Semiconductors,* edited by J. K. Furdyna and J. Kossut, Vol. 25 in Series on Semiconductors and Semimetals (Academic, New York, 1988).
[7]J. K. Furdyna, J. Appl. Phys. **64**, R29 (1988).
[8]G. A. Sefler, E. Oh, R. S. Rana, I. Miotkowski, A. K. Ramdas, and D. D. Nolte, Opt. Lett. **17**, 1420 (1992).
[9]J. Strait and A. M. Glass, in *Photorefractive Materials and Their Applications I* (Springer-Verlag, Berlin, 1989).
[10]R. B. Bylsma, P. M. Bridenbaugh, D. H. Olson, and A. M. Glass, Appl. Phys. Lett. **51**, 889 (1987).
[11]J. A. Gaj, J. Ginter, and R. R. Galazka, Phys. Status Solidi B **89**, 655 (1978).
[12]D. U. Bartholomew, J. K. Furdyna, and A. K. Ramdas, Phys. Rev. B **34**, 6943 (1986).
[13]E. Oh, D. U. Bartholomew, A. K. Ramdas, J. K. Furdyna, and U. Debska, Phys. Rev. B **44**, 10 551 (1991).
[14]E. D. Palik and B. W. Henvis, Appl. Opt. **6**, 603 (1967).
[15]W. Voigt, Ann. Phys. (Leipzig) **1**, 389 (1900).
[16]J. Strait, J. D. Reed, and N. V. Kukhtarev, Opt. Lett. **15**, 209 (1990).
[17]G. C. Valley, J. Appl. Phys. **59**, 3363 (1986).
[18]F. P. Strohkendl, J. M. C. Jonathon, and R. W. Hellwarth, Opt. Lett. **11**, 312 (1986).
[19]A. V. Komarov, S. M. Ryabchenko, O. V. Terletskii, I. I. Zheru, and R. D. Ivanchuk, Zh. Eksp. Teor. Fiz. **73**, 608 (1977) [Sov. Phys. JETP **46**, 318 (1977)].
[20]E. Oh, D. U. Bartholomew, and A. K. Ramdas, Phys. Rev. B **38**, 13 (1988).
[21]P. M. Johansen and A. K. Jensen, J. Opt. Soc. Am. B **8**, 2342 (1991).
[22]D. D. Nolte and A. M. Glass, Opt. Quantum Electron. **22**, S47 (1990).
[23]D. D. Nolte, D. H. Olson, and A. M. Glass, Appl. Phys. Lett. **56**, 163 (1990).
[24]R. S. Rana, R. Steldt, E. M. Monberg, and D. D. Nolte, J. Opt. Soc. Am. B **9**, 1614 (1992).
[25]D. D. Nolte, D. H. Olson, and A. M. Glass, Phys. Rev. Lett. **63**, 891 (1989).
[26]M. C. Bashaw, T. Ma, R. C. Barker, S. Mroczkowski, and R. R. Dube, Phys. Rev. B **9**, 1666 (1990).
[27]M. C. Bashaw, T. Ma, R. C. Barker, S. Mroczkowski, and R. R. Dube, J. Opt. Soc. Am. B **7**, 2329 (1990).
[28]R. S. Cudney, R. M. Pierce, G. D. Bacher, and J. Feinberg, J. Opt. Soc. Am. B **8**, 1326 (1991).
[29]A. A. Kamshilin, Opt. Commun. **93**, 350 (1992).
[30]C. H. Kwak, S. Y. Park, H. K. Lee, and E.-H. Lee, Opt. Commun. **79**, 349 (1990).
[31]R. B. Bylsma, D. H. Olson, and A. M. Glass, Opt. Lett. **13**, 853 (1988).
[32]R. M. Pierce, R. S. Cudney, G. D. Bacher, and J. Feinberg, Opt. Lett. **15**, 414 (1990).

[33]K. V. Shcherbin, R. V. Litvinov, and E. S. Shandarov (unpublished).
[34]K. Walsh, T. J. Hall, and R. E. Burge, Opt. Lett. **12**, 1026 (1987).
[35]Q. N. Wang, R. M. Brubaker, D. D. Nolte, and M. R. Melloch, J. Opt. Soc. Am. B **9**, 1626 (1992).
[36]J. E. Millerd, S. D. Koehler, E. M. Garmire, A. Partovi, A. M. Glass, and M. B. Klein, Appl. Phys. Lett. **57**, 2776 (1990).